RSC Advances

ROYAL SOCIETY OF CHEMISTRY

www.rsc.org/advances

The actual potential distributions inside cavities under gas evolution and film formation conditions

X.T. Sun[a,*], H.S. Lin [b], X.S. Chen[a], C.Y. Zhang[a], R.X. Du[a]

[a] Center for Precision Engineering, Guangzhou Institute of Advanced Technology Chinese Academy of Sciences, Guangzhou 511458, China

[b] Guangdong Technical College of Water Resources and Electric Engineering, Guangzhou 510925, China

Abstract

The non-uniform distribution of the electrode potential within submerged cavities is an important consideration in understanding the mechanisms of various electrochemical processes. In the present paper, the actual potential distributions inside cavities have been measured under conditions of gas evolving and oxide film formation on titanium electrodes in neutral media using scanning micro-reference electrode technique. The experimental results show that the bubbles motion and films growth inside cavities which differ greatly from that on flat or vertical electrodes, exert substantial effects on the potential distribution characteristic. The anomalous high-amplitude of potential variation and the unexpected local potential increase in the bottom part of cavities caused by the coalescing bubble covering cavities has been experimentally revealed. Moreover, under oxide film formation, once the completed oxide film is generated, the potential and current will be redistributed inside cavities. By improving the upper surface coarseness, a uniform potential distribution inside cavities can be achieved.

Keywords: Potential distribution; cavity; micro-reference electrode; hydrogen evolution; film formation

1. Introdution

A metal surface with a submerged cavity, often happens under the conditions of cathodic protection [1], electrodepositing [2], electrocoagulation technology [3] and local corrosion process [4, 5]. The presence of cavities strongly accentuates the spatial non-uniformity of the potential and current distributions on the metal surface and inside the depth of the cavity. Moreover, under gas evolution or film formation/deposition, the presence of growing bubbles or films greatly affects

Corresponding author. Tel.:+86 20 22912753; Fax: +86 20 22912601; E-mail: xt.sun@giat.ac.cn

the current-potential characteristics of an electrochemical cell. The additive effects, namely the gas evolution or film formation occurring inside cavities, can lead to some unexpected potential distribution characteristics highlighted in this study.

During operation of gas-evolving electrodes, bubble growth shields the active electrochemical surface of the working electrode and after detachment of the bubble a compensating flow towards the electrode occurs, which are known to have a major effect on overpotential and current density [6-8]. The electrode overpotential is usually expressed in terms of partial components related to ohmic, activation and concentration effects. For gas-evolving electrodes, the concentration overpotential component mainly refers to the concentration profile of dissolved gases at the electrode surfaces. In the previous studies [9-11], it was shown that the dissolved-gas concentration component acts as a compensation term to the ohmic and activation losses since the departure of a bubble makes the screened surface free to react. Under certain conditions, the concentration overpotential could be the dominant component. However the previous theoretical analyses or numerical calculations based on the flat or vertical electrodes [12-14] are unconcerned with the submerged cavity electrode. There is few works concerning the effect of gas-evolving behavior on the electrochemical processes inside the submerged cavity electrode.

Moreover, for the film-formation/deposition electrodes, the growing films accentuate the ohmic effect on the potential distribution inside cavities due to the high solid phase resistivity. It is known that when the current lower than the limiting current, the ohmic effect associated with electrode-surface screening by film-formation/deposition is the predominant component [2, 4, 15-17]. It can be predicted that the cavity wall surface conditions will play an important role in the potential distribution inside cavities, but which remained unverified experimentally.

This study is focused on the actual potential distributions caused by the gas bubble evolving and oxide film formation inside cavities from a new perspective. The analysis is based on a set of experiments scanning potential distributions inside the artificial cavies of titanium electrode in neutral NaCl solution under current control. It can be seen that with the coalescing bubble covering the cavity, the bubbles rising upwards effectively lead to an unexpected local overpotential increase at the bottom of cavities. Moreover, it also shows that under the oxide film formation, by improving the upper surface coarseness, a more uniform potential distribution inside cavities can be achieved.

2. Experiments

2.1 Sample preparation

Commercially pure titanium grade 2 rods of Φ 7 mm×12 mm were used as the specimens. The investigated cavity with a diameter 2 mm and a depth 10 mm was drilled in the middle surface of cylindrical specimens. The remaining surfaces were insulated from the electrolyte by a thermosetting resin. The solutions of 1% and 5% aqueous NaCl were prepared from analytical reagent grade chemicals and distilled water. The sand blasting treatment was carried out with a laboratory sand-blasting machine at 0.8 MPa. The blasting particles were SiC-particles of 200 μm mean size. Surface roughness values were measured with a contact profilometer (SJ-210, Mitutuyo, Japan).

2.2 Microelectrochemical setup

The setup for microelectrochemical investigations based on the micro-reference electrode is shown schematically in Fig.1. The typical three-electrode cell was used. A Unisense micro-reference electrode REF-10 (silver/silver-chloride) with the outside tip diameter 8-12 μm was fixed in the holder of MM33 micromanipulator mounted on a heavy laboratory stand. The micromanipulator can position the micro-reference electrode with the z-axis (depth) precision of 10 microns, while the x- and y-axis precision of 100 microns. A platinum counter-electrode was processed into L-shape with a round cavity in the middle to allow the microcapillary pass through. The test cell was fixed at the heavy laboratory stand. The distance between the working electrode and counter electrode was set as 5mm.

2.3 Scanning methods

All scanning measurements were performed in constant current mode using a CHI660D potentiostat. The typical current densities and solution concentrations were chosen according to the results of potentiodynamic curves carrying out on the flat surface of specimens. For the measurement of the potential variation between cavities opening and bottom, the monitoring time at each location was set as 500 seconds. Considering the result comparability and the test duration, the monitoring time for the measurement of the potential distribution at every millimeter was set as 50 seconds. Each potential-time monitoring experiment was repeated at least three times, with a fresh specimen being used for each test.

3. Results and discussion

3.1 Potential distribution analysis under gas evolution during cathodic polarization

To minimize the interference of the microcapillary to the local electrochemical microenvironment and the force balance of the wall-attached bubbles, the total potential variation within the 10mm-depth cavity were measured (see Fig. 2) in 1% and 5% NaCl at cathodic current densities of 10^{-4} and 10^{-3} A/cm^2. The reason for choosing cathodic 10^{-4} and 10^{-3} cm^2 as current densities is to reduce the effect of the presence of dissolved oxygen on hydrogen overpotential. At 10^{-4} and 10^{-3} A/cm^2 that are greater than ten times I_d of oxygen, the presence of dissolved oxygen has little effect on hydrogen overpotential [18].

Figure 2a and 2c show the regular "square wave" feature, indicating the measured potential variation amplitude between the cavity opening and bottom was unchanged in the experimental period. It can be observed that the small H_2 bubbles rise upwards from the cavities. In 1% NaCl the variation amplitudes are about 50 and 200 mV at 10^{-4} and 10^{-3} A/cm^2 respectively. In 5% NaCl the potential variation amplitudes are about 10 mV and 100 mV for 10^{-4} and 10^{-3} A/cm^2 respectively. The total potential variations inside cavities are proportional to the electrolyte and polarization resistances. The net effect of the hydrogen evolution is the expected overpotential decrease [7, 8].

It is noted that "anomalous" potential variations at 10^{-3} A/cm^2 in 1% and 5% NaCl solutions can reach about 700-800 mV, due to the coalescing bubble covering the cavity opening. This bubble motion is special to the cavity electrode contrasting to the flat or vertical electrodes [19]. At different solution concentrations and current densities, the potential variation amplitudes caused by the sudden birth and departure of this particular bubble are close.

The potential distribution profiles within the 10mm-depth cavity in 1% NaCl at 10^{-3} and 10^{-2} A/cm^2 are measured comparatively (see Fig. 3). The more interference of micro-probe helps the bubbles to detach. The maximum potential variation amplitude decreases from about 800 mV to 500 mV (Fig. 3a). Moreover, Fig. 3a Ⅰ shows that at the initial stage without the visible coalescing bubble, two zones are distinguished: (a zone) the overpotential quickly decreases up to 80% of total drop (to -1.48 V), corresponding to where from the cavity opening to the depth of 4mm; and (b zone) the overpotential almost constant, corresponding to where from 4mm depth to the cavity bottom. If only considering the primary current distribution, the cavity upper surface has the higher current density, which leads to higher H_2 release rate and lower H_2 coverage

fraction [6]. Meanwhile, this higher H_2 release rate has a corresponding counterpart: although the departures of small bubbles make the covered surface free to react, which locally enhances the gas production reaction, the increasing gas concentration in the adjacent region would decrease the electrolyte conductivity so that decreasing local current density. The extent depends on the bubbles release rate and the H_2 evolution rate. Without the coalescing bubble covering the cavity, the detaching bubbles can easily escape from the cavity. In this circumstance, the net effect of the H_2 bubble evolution is that the overpotential decrease with the depth increasing. The process is schematically depicted in Fig. 3b Ⅰ.

With the appearance of the bubble (Fig. 3a Ⅱ), also the two zones are distinguished: (a zone) the overpotential rapidly drops to the minimum values and then (b zone) rises slowly with the cavity depth increasing. This unexpected local increase can be explained by the change of covered surface area adhered by bubbles inside cavities. With the large coalescing bubble covering the cavity opening, the small detaching bubbles collect on the gas-liquid interface (as depicted in Fig. 3b Ⅱ, Ⅲ). This process depends on the bubbles coalescence frequency and the H_2 evolution rate. The bigger the coalescing bubble on the cavity opening grows, the greater electrode surface area would be covered. To maintain the constant current, there is an increase in current density at the bottom part of the cavity. In this circumstance, the bubbles collecting at the upper surface tend to compensate or even overpass the geometry effect on the current/potential distribution. It should be noted that this local enhancement of cavity bottom potential is still associated with the ohmic effect which is caused by the screening of bubbles attached on upper internal surface of the cavity, but not results from the dissolved-gas concentration effect which is caused by the exposure of screened bottom surface to the solution, as pointed out by previous research on the flat electrode [7].

At 10^{-2} A/cm^2 (Fig.3c), due to the larger current density, hydrogen evolution was expected to be more intense than at 10^{-3} A/cm^2. The coalescing bubble attached to the cavity opening is not observed. The potential distribution behavior at 10^{-2} A/cm^2 shows that two zones are less distinguished: (a zone) where the overpotential quickly decreases up to 80% of total drop (to -1.55 V); and (b zone) where the overpotential keeps decreasing (to -1.45 V) but slowly. The use of higher current densities improves the effective electrode thickness inside cavities as expected, however this improvement is particularly associated with the situation without coalescing bubble covering cavity opening.

3.2 Potential distribution analysis under film formation during anodic polarization

The total anodic potential variation within the 10mm-depth cavity were measured in 1% and 5% NaCl solutions at current densities of 10^{-5} and 10^{-4} A/cm^2 (see Fig. 4). The curves show that the potential increases rapidly with time until a constant potential is reached, at which point oxygen is evolved [18].

At 10^{-5} A/cm^2 (see Fig. 4a, c) the potential variation amplitudes are constant and approximately the same in 1% and 5% NaCl solutions, being 5mV. Also, the oxygen evolution potential is approximately the same in 1% and 5% NaCl solutions, being +1.45 volts. It should be noted that there is no anomalous potential variation associated with the coalescing bubble due to the less intense evolution. At 10^{-4} A/cm^2 in 1% NaCl solution (seen in Fig. 4b) after reaching the oxygen evolution value, the cavity opening potential E_o increases slowly but remains within +2 volts. The potential variation amplitude rises slowly also from 40mV to 50mV with time increasing. Previous investigations [18] have shown that the cessation of oxygen evolution occurs at about +2 V, after which all current are available to form TiO_2. Under the experimental conditions in Fig. 4a-c, small bubbles can be observed to rise upwards from the cavity at a lower rate. The results are in good agreement with literature data.

In higher solution concentration of 5% NaCl at 10^{-4} A/cm^2 (see Fig. 4d), there is an obvious dividing point at about +2 volts separating the slowly increasing and the rapidly increasing E_o. During the slow potential E_o increasing, the potential variation amplitude is about 30 mV, slightly lower than the value measured in 1% NaCl solution. It should be noted that during the rapid E_o increasing, the total potential variation within the cavity is rapidly enlarged to about +8 volts. This can be accounted for the completed oxide film formation on the opening cavity surface. In this stage, almost all of the applied current is used to form and thicken oxide films, and thus the surface within cavity has very low distributed currents. Namely, once the completed oxide film is generated, the potential and current will be redistributed. As the oxide film thickens rapidly, the potential at the cavity bottom decreases to about +1.42 volts, which is expected to further decrease with the E_o increasing.

To verify whether the incomplete film formation would result in a different potential distribution characteristic inside the cavity, the specimens are treated by a large grit sand-blasting process, which leads to a macro-roughness (Ra = 4.24 ± 0.08 μm) of specimens surface. Then the same test as Fig. 4d was repeated in the sandblasted specimens. Compared with Fig. 4d, the high-amplitude variation of overpotential does not appear in the Fig. 5. However, Fig. 5 shows similar dividing

point at about +2 volts. Differently, the potential E_o quickly goes through the slowly and rapidly increasing stages. During the rapid E_o rise, the total potential variation within the cavity is only a few hundred millivolts. The sandblasting treatments increase the surface roughness and cause the higher growth rate and more defects on oxide films. Hence, the incomplete film causes the locally-depressed ohmic and activation overpotentials, and more uniform potential distribution. This experimentally confirms that cavity surface condition has a strong effect in the potential and current distributions inside cavities.

4. Conclusion

The results showed that under the hydrogen evolution, the potential current characteristics inside cavity vary greatly with the sudden birth, growth and detachment of the coalescing bubble covering the cavity opening. During this period, the bubbles rising upwards and aggregation at gas-liquid interface tend to compensate the primary current/potential distribution. Given the applied current lower than the limiting current, the formation of oxide film with the enough high ohmic resistance is the key effect on the potential distribution inside cavity. In this work, by depressing the resistance of oxide film formed on upper surface, namely by improving the upper surface coarseness, a more uniform potential distribution inside cavities was achieved. These potential distribution characteristics may facilitate or, perhaps, prevent any actual electrochemical process inside the submerged cavity. The scanning micro-probe reference electrode technique was proven to be effective for the potential measurements inside cavities under extreme operation conditions.

Acknowledgments

This research was supported by the National Natural Science Foundation of China (Nos. 51001050) and the Program of the Pearl River Young Talents of Science and Technology in Guangzhou (No.2013J2200009).

Reference

[1] M.H. Parsa, S.R. Allahkaram and A.H. Ghobadi, *J. Pet. Sci. Eng.* 2010,**72**, 215 .

[2] S. Jung, M. D. Gross, R. J. Gorte and J. M. Vohs, *J. Electrochem. Soc.* 2006, **153**, 1539.

[3] A. Vázquez, I. Rodríguez and I. Lázaro, *J. Chem. Eng.* 2012, **179**, 253.

[4] H.W. Pickering, *Mater. Sci. Eng. A.* 1995, **198**, 213.

[5] X.T. Sun, Z.X. Kang, X.L. Zhang, H.J. Jiang, R.F. Guan and X.P. Zhang, *Electrochim. Acta.* 2011, **56**, 6389.

[6] H. Vogt, *Electrochim. Acta.* 2012, **78**, 183.

[7] C. Gabrielli, F. Huet and R. P. Nogueira, *Electrochim. Acta.* 2005, **50**, 3726.

[8] C. Brussieux, Ph. Viers, H. Roustan and M. Rakib, *Electrochim. Acta.* 2011, **56**, 7194.

[9] M. Philippe, H. Jérôme, B. Sebastien and P. Gérard, *Electrochim. Acta.* 2005, **51**, 1140.

[10] S. Kawai, Y. Fukunaka and S. Kida, *J. Electrochem. Soc.* 2010, **157**, 40.

[11] M. M. Saleh, J. W. Weidner and B. G. Ateya, *J. Electrochem. Soc.* 1995, **142**, 4113.

[12] R. Wüthrich, Ch. Comninellis and H. Bleuler, *Electrochim. Acta.* 2005, **50**, 5242.

[13] J. Eigeldinger and H. Vogt, *Electrochim. Acta.* 2000, **45**, 4449.

[14] H. Vogt and R.J. Balzer, *Electrochim. Acta.* 2005, **50**, 2073.

[15] J. L. Nava, M.T. Oropeza, C. Ponce de León, J. González-García and A.J. Frías-Ferrer, *Hydrometallurgy.* 2008, **91**,98.

[16] G. S. Kim, T. Merchant, J. D. Urso, L. A. Gochberg and K. F. Jensen, *J. Electrochem. Soc.* 2006, **153**,761.

[17] S. Haber and L. Gal-Or, *J. Electrochem. Soc.* 1992, **139**, 1071.

[18] C. D. Hall and N. Hackerman, *J. Electrochem. Soc.* 1953, **57**, 262.

[19] Steven Lubetkin, *Electrochim. Acta.*2002, **48**, 357.

Figure Captions

Fig.1 Experimental setup for the cavity microelectrochemical scanning investigations.

Fig.2 Potential variations inside the 10mm-depth cavity in titanium electrode measured in 1% (a, b) and 5% (c, d) NaCl at cathodic current densities of 10^{-4} (a, c) and 10^{-3} (b, d) A/cm^2.

Fig.3 Potential distributions inside the 10mm-depth cavity in titanium electrode measured in 1% NaCl at cathodic current densities of (a) 10^{-3} and (c) 10^{-2} A/cm^2; (b) graphical illustration of the effect of bubbles motion on the potential distributions corresponding to (a) Ⅰ, Ⅱ and Ⅲ processes.

Fig.4 Potential variations inside the 10mm-depth cavity in titanium electrode measured in 1% (a, b) and 5% (c, d) NaCl at anodic current densities of 10^{-5} (a, c) and 10^{-4} (b, d) A/cm^2.

Fig.5 Potential variations inside the 10mm-depth cavity in sandblasted titanium electrode measured in 5% NaCl at anodic current densities of 10^{-4} A/cm^2.

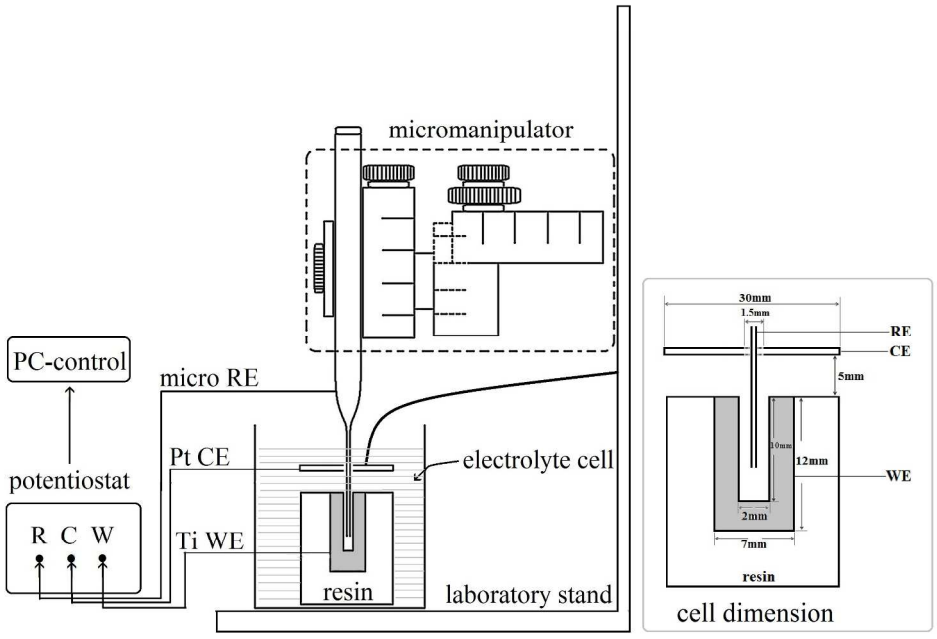

Fig.1 Experimental setup of the cavity microelectrochemical scanning investigations.
787x558mm (96 x 96 DPI)

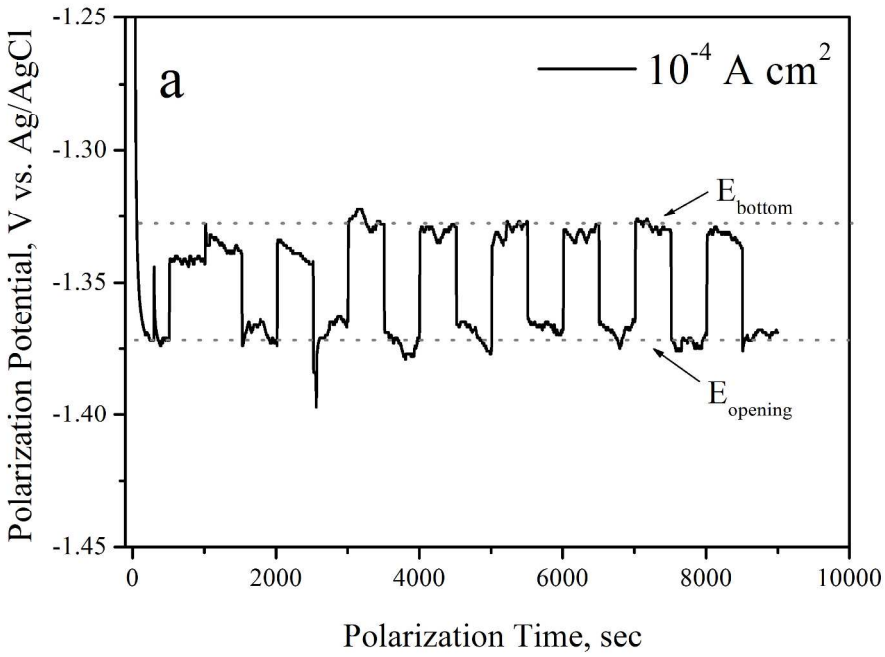

Fig. 2a Potential variations inside the 10mm-depth cavity in titanium electrode measured in 1% (a, b) and 5% (c, d) NaCl at cathodic current densities of 10-4 (a, c) and 10-3 (b, d) A/cm2.
270x214mm (300 x 300 DPI)

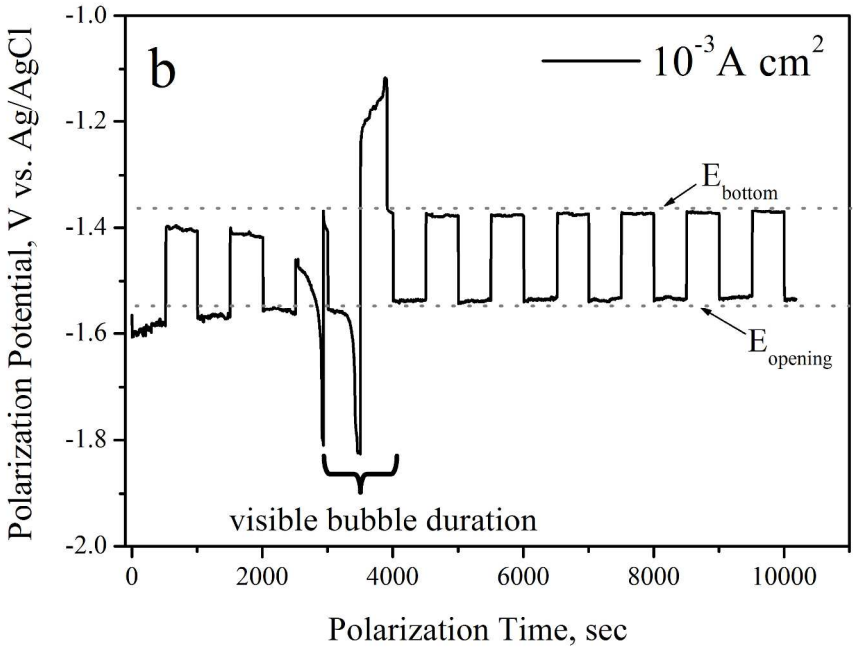

Fig. 2b Potential variations inside the 10mm-depth cavity in titanium electrode measured in 1% (a, b) and 5% (c, d) NaCl at cathodic current densities of 10-4 (a, c) and 10-3 (b, d) A/cm2.
270x213mm (300 x 300 DPI)

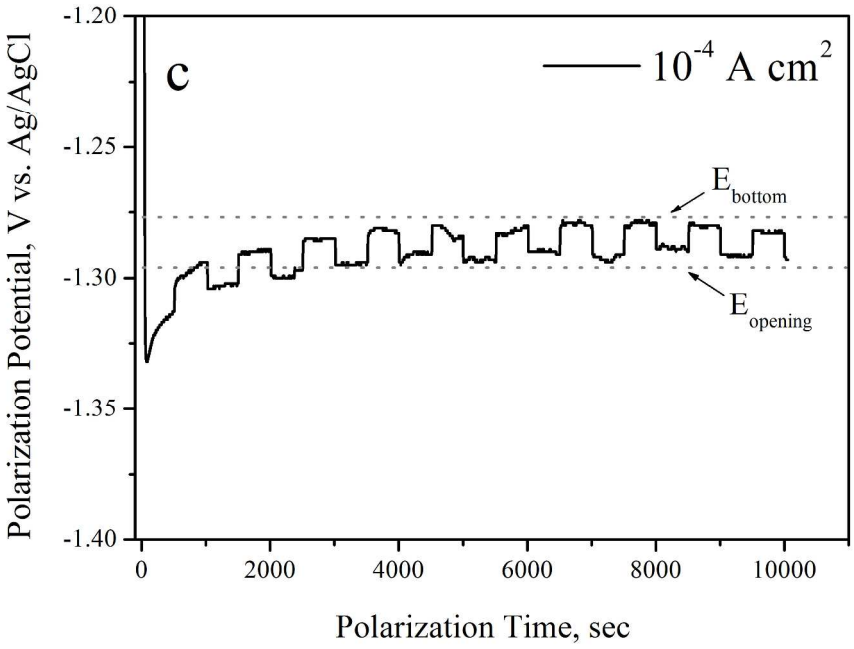

Fig. 2c Potential variations inside the 10mm-depth cavity in titanium electrode measured in 1% (a, b) and 5% (c, d) NaCl at cathodic current densities of 10-4 (a, c) and 10-3 (b, d) A/cm2.
273x214mm (300 x 300 DPI)

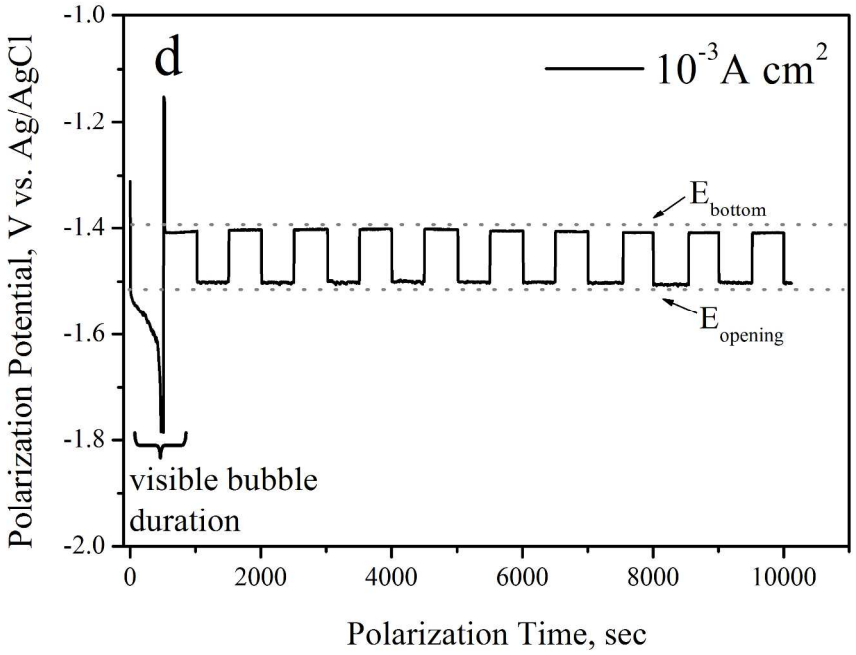

Fig. 2d Potential variations inside the 10mm-depth cavity in titanium electrode measured in 1% (a, b) and 5% (c, d) NaCl at cathodic current densities of 10-4 (a, c) and 10-3 (b, d) A/cm2.
270x214mm (300 x 300 DPI)

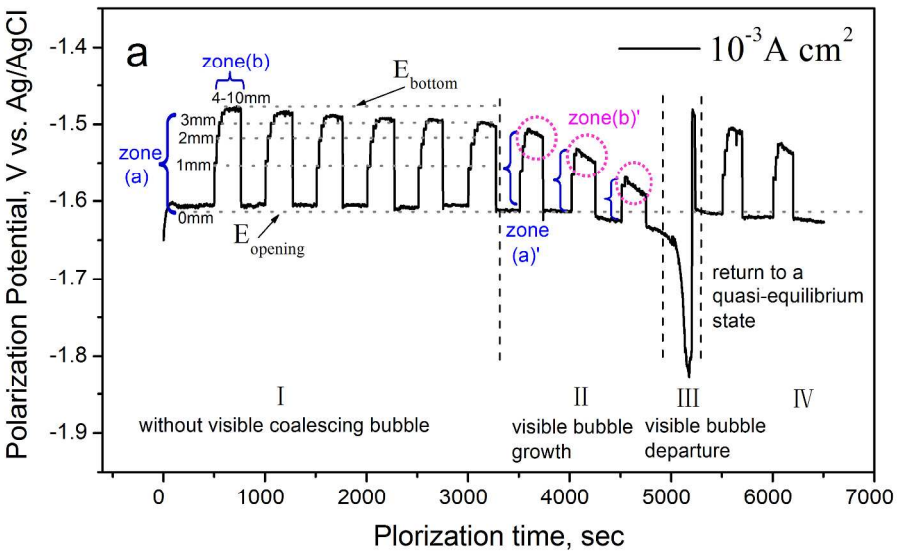

Fig. 3a Potential distributions inside the 10mm-depth cavity in titanium electrode measured in 1% NaCl at cathodic current densities of (a) 10-3 and (c) 10-2 A/cm2; (b) graphical illustration of the effect of bubbles motion on the potential distributions corresponding to (a) Ⅰ, Ⅱ and Ⅲ processes.
324x207mm (300 x 300 DPI)

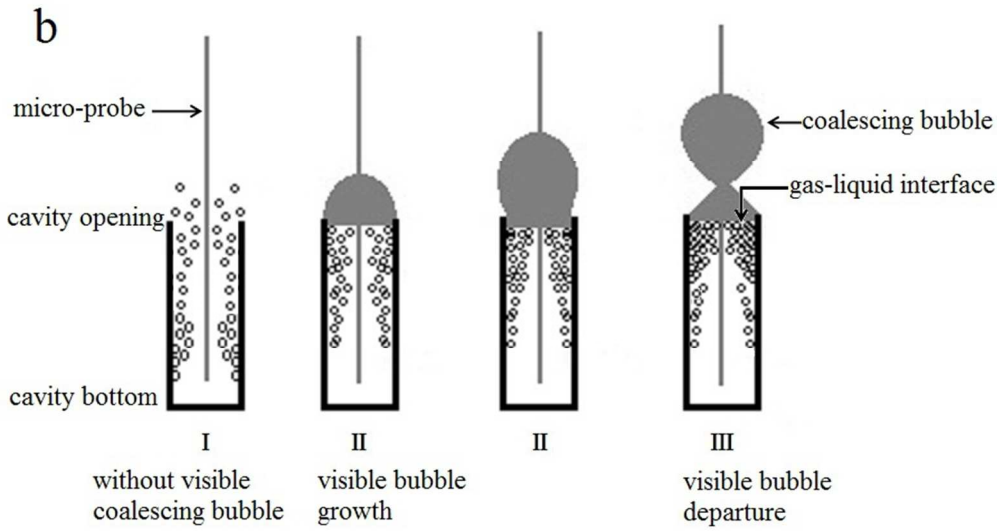

Fig. 3b Potential distributions inside the 10mm-depth cavity in titanium electrode measured in 1% NaCl at cathodic current densities of (a) 10-3 and (c) 10-2 A/cm2; (b) graphical illustration of the effect of bubbles motion on the potential distributions corresponding to (a) Ⅰ, Ⅱ and Ⅲ processes.
236x133mm (96 x 96 DPI)

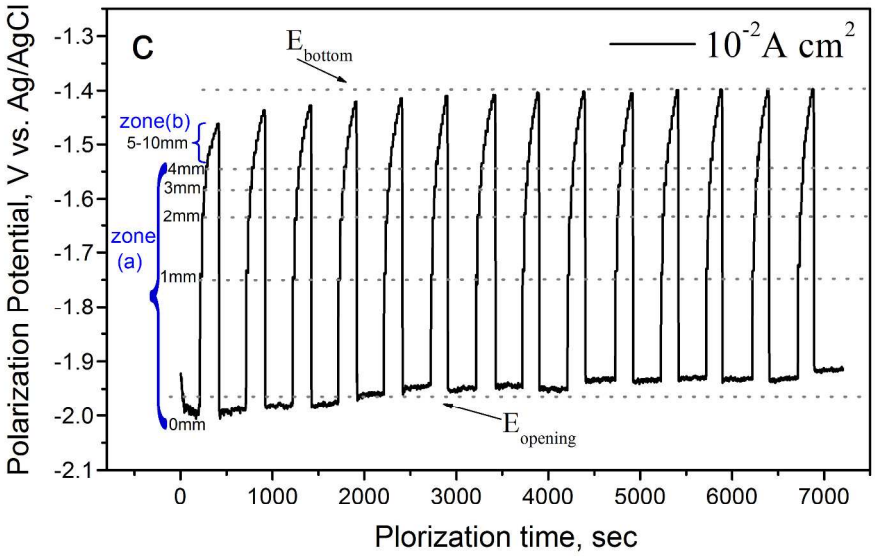

Fig. 3c Potential distributions inside the 10mm-depth cavity in titanium electrode measured in 1% NaCl at cathodic current densities of (a) 10-3 and (c) 10-2 A/cm2; (b) graphical illustration of the effect of bubbles motion on the potential distributions corresponding to (a) Ⅰ, Ⅱ and Ⅲ processes.
311x211mm (300 x 300 DPI)

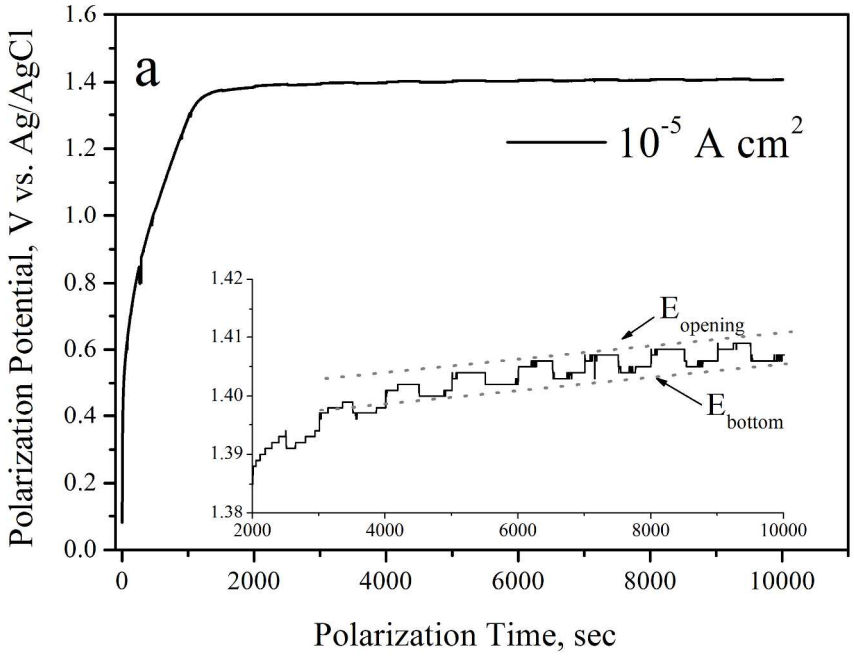

Fig. 4a Potential variations inside the 10mm-depth cavity in titanium electrode measured in 1% (a, b) and 5% (c, d) NaCl at anodic current densities of 10-5 (a, c) and 10-4 (b, d) A/cm2.
267x213mm (300 x 300 DPI)

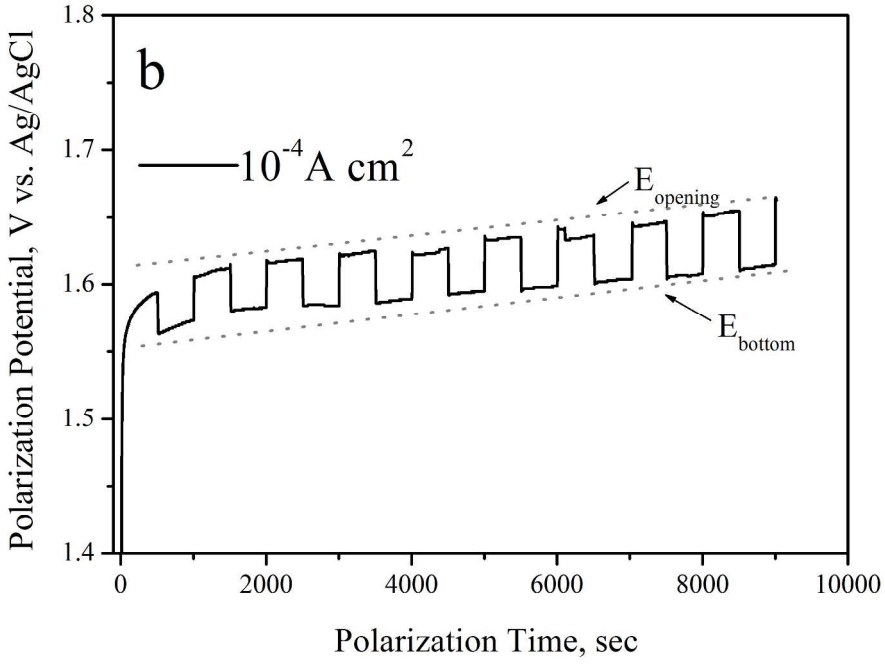

Fig. 4b Potential variations inside the 10mm-depth cavity in titanium electrode measured in 1% (a, b) and 5% (c, d) NaCl at anodic current densities of 10-5 (a, c) and 10-4 (b, d) A/cm2.
266x213mm (300 x 300 DPI)

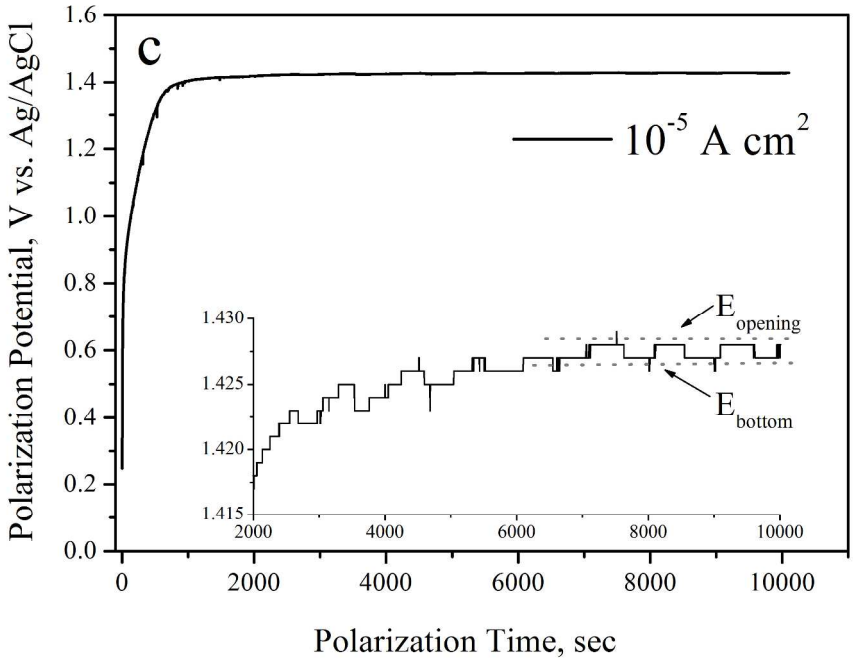

Fig. 4c Potential variations inside the 10mm-depth cavity in titanium electrode measured in 1% (a, b) and 5% (c, d) NaCl at anodic current densities of 10-5 (a, c) and 10-4 (b, d) A/cm2.
267x214mm (300 x 300 DPI)

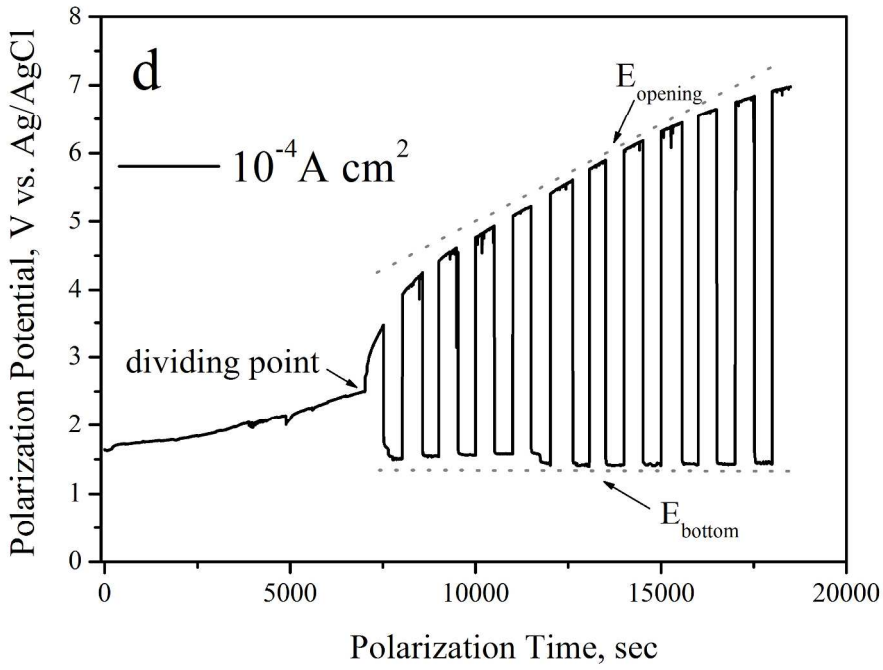

Fig. 4d Potential variations inside the 10mm-depth cavity in titanium electrode measured in 1% (a, b) and 5% (c, d) NaCl at anodic current densities of 10-5 (a, c) and 10-4 (b, d) A/cm2.
262x213mm (300 x 300 DPI)

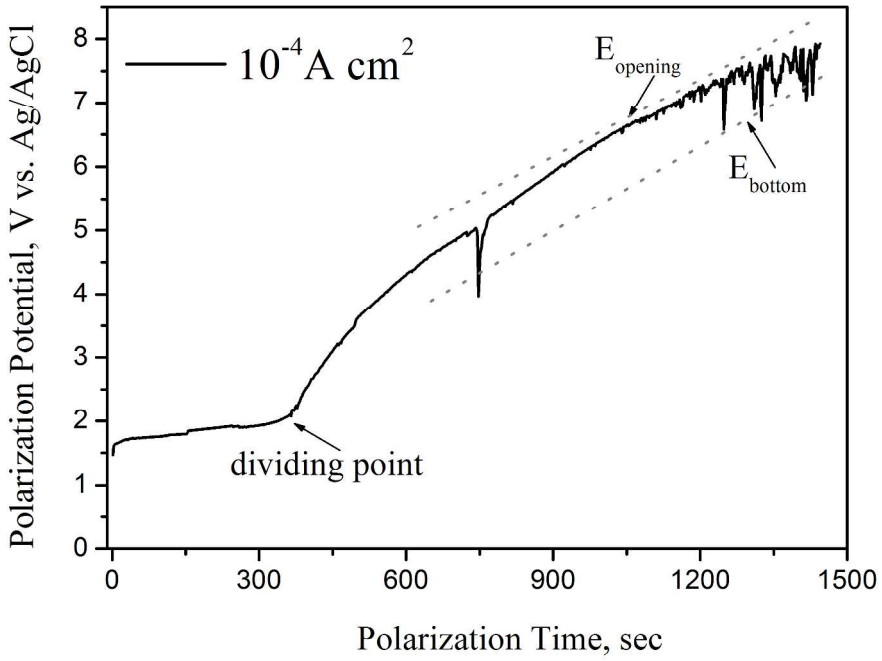

Fig. 5 Potential variations inside the 10mm-depth cavity in sandblasted titanium electrode measured in 5% NaCl at anodic current densities of 10-4 A/cm2.
264x214mm (300 x 300 DPI)